JOURNAL OF CATALYSIS 149, 127–141 (1994)

Production of Olefins by Oxidative Dehydrogenation of Propane and Butane over Monoliths at Short Contact Times[1]

M. Huff[2] and L. D. Schmidt[3]

Department of Chemical Engineering and Materials Science, University of Minnesota, Minneapolis, Minnesota 55455

Received February 15, 1994; revised June 2, 1994

The autothermal production of olefins from propane or *n*-butane by oxidative dehydrogenation and cracking in air or oxygen at atmospheric pressure over noble metal coated ceramic foam monoliths at contact times of ~5 milliseconds has been studied. On Pt, synthesis gas (CO and H_2) dominates near its stoichiometry, while olefin production dominates at higher fuel-to-oxygen ratios. No carbon buildup is observed, and catalysts exhibit no deactivation over at least several days. On Rh, primarily synthesis gas is produced under these conditions, while on Pd, carbon deposition rapidly deactivates the catalyst. We observe up to 65% selectivity to olefins at nearly 100% conversion of propane or *n*-butane with a catalyst contact time of 5 ms. Ethylene selectivity is maximized by increasing the reaction temperature, either by preheating the reactants or by using oxygen enriched air. Propylene selectivity is maximized by lower temperature and shorter catalyst contact time. Very small amounts of alkanes and higher molecular weight species are obtained, suggesting that a homogeneous pyrolysis mechanism is not occurring. A very simple reaction mechanism appears to explain the observed product distribution. Reactions are initiated by oxidative dehydrogenation of the alkane by adsorbed oxygen to form a surface alkyl. On Pt, β-hydrogen and β-alkyl elimination reactions of adsorbed alkyl dominate which lead to olefin production rather than cracking to C_s and H_s. © 1994 Academic Press, Inc.

INTRODUCTION

The abundant supplies of liquefied petroleum gas, predominantly propane and butanes, offer enticing routes to short chain olefins and thus to chemical feedstocks and liquid fuels (1). Current practice produces ethylene, propylene, and butylenes from ethane, propane, and butane by thermal pyrolysis with high temperatures required by equilibrium considerations. Coking is often a problem in thermal pyrolysis, and steam is usually added to the fuel to reduce carbon deposition. Hence, this process is often called steam cracking.

[1] This research was partially supported by DOE under Grant DE-FG02-88ER13878-AO2.

[2] Supported by DARPA-NDSEG Graduate Fellowship.

[3] To whom correspondence should be addressed.

We have recently reported that ethylene formation by catalytic oxidative dehydrogenation of ethane over Pt-coated monoliths yields up to 70% selectivity to ethylene at more than 80% conversion of ethane with a catalyst contact time of only 5 ms with no carbon formation (2). This very short contact time potentially allows the use of reactors 100 to 1000 times smaller than those currently used for the same ethylene yield. Also, unlike the thermal pyrolysis reactor, which must be externally heated, the catalytic oxidative dehydrogenation reactor operates autothermally and nearly adiabatically (at ~1000°C), thus further reducing operating costs.

In this paper, oxidation over monoliths is applied to the conversion of propane and *n*-butane to olefins. The possible reactions of propane and *n*-butane are listed in Tables 1 and 2 with their corresponding heats of reaction and equilibrium constants. The reactants and products can also react to form solid carbon, C_S. These reactions are listed in Table 3. The reactions in the tables are numbered and will be referenced by these numbers in the text.

Our objective is to determine under what conditions olefin production can be maximized over noble metal coated monolithic catalysts. We have found that Pt is the preferred catalyst for olefin production, but the performance of Rh and Pd coated catalysts will also be discussed briefly.

Conversion of Propane and n-Butane to Olefins

Propylene and ethylene are formed from propane homogeneously by thermal pyrolysis (3, 4) and heterogeneously by oxidative dehydrogenation and cracking over oxide catalysts (1, 5–7). Thermal pyrolysis of propane (Eqs. [4] and [5]) typically leads to approximately 40% selectivity to ethylene and 20% selectivity to propylene at 80% conversion of propane (3) (all selectivities indicated are based on carbon atoms). The reactor must be heated to 800°C, and maximum (near equilibrium) olefin yield is achieved at residence times ≥0.3 s.

Because this process consumes energy and is limited by equilibrium, oxidative dehydrogenation of propane

0021-9517/94 $6.00

TABLE 1

Reactions of Propane

			% C_3H_8 in air	ΔT_{ad} (°C)	C_3H_8/O_2	$\Delta H°$ (kJ/mol)	K_{eq} 1200 K
[1]	$C_3H_8 + 5O_2 \rightarrow 3CO_2 + 4H_2O$	Complete combustion	4.0	2800	0.20	−2043	$>10^{38}$
[2]	$C_3H_8 + \frac{3}{2}O_2 \rightarrow 3CO + 4H_2$	Partial oxidation to syngas	12.3	900	0.67	−227	$>10^{38}$
[3]	$C_3H_8 + \frac{1}{2}O_2 \rightarrow C_3H_6 + H_2O$	Oxidative dehydrogenation	29.6	1044	2.00	−118	3.5×10^9
[4]	$C_3H_8 \rightarrow C_3H_6 + H_2$	Dehydrogenation	—	—	—	+124	4.4×10^1
[5]	$C_3H_8 \rightarrow C_2H_4 + CH_4$	Cracking	—	—	—	+83	3.1×10^3

(Eq. [3]) has also been investigated extensively (1, 5–9). This process has been found to be quite selective (~65% propylene) over V–Mg–O catalysts at very low conversion (<15%), but the selectivity quickly decreases at higher conversions. At 20% propane conversion, the propylene selectivity is already reduced to only 40% (5). This trade-off between selectivity and conversion severely limits the value of this process. It was suggested that the mechanism of this process involves both homogeneous and heterogeneous reactions (5, 7). Since these processes are operated under fuel-rich conditions ($C_3H_8/O_2 \approx 0.5$), carbon deposition (Eqs. [13]–[16]) and consequent catalyst deactivation can still be a problem. For this reason, in previous experiments the reactants were diluted in He or N_2 (typical feed compositions are $C_3H_8 : O_2 : N_2$ of 1 : 2 : 10) (5), and the reaction took place at fairly low temperatures (500–600°C) where coke formation was minimal.

Olefins are also formed from *n*-butane both by homogeneous pyrolytic routes (10, 11) and by heterogeneous oxidative dehydrogenation and cracking over oxide catalysts (12, 13). Thermal pyrolysis of *n*-butane (Eqs. [10]–[12]) gave ~50% selectivity to propylene and ~20% selectivity to ethylene (10) at ~40% *n*-butane conversion (11) when the reactor was heated to ≥750°C for the endothermic reactions (Eqs. [10]–[11]) to proceed to equilibrium (see Table 4). The remainder of the products were 20% CH_4 and 10% C_2H_6. At higher temperatures, higher *n*-butane conversion was achieved (75–95%), but at the expense of the propylene selectivity, which dropped below 25% (14). At these higher conversions, more high-molecular-weight species (C_4+) are produced. In both of these cases, carbon deposition must be controlled by adding steam to the hydrocarbon feed.

Oxidation of *n*-butane to olefins (Eqs. [8]–[9]) over oxide catalysts has also been investigated. Fairly high selectivities to butylene (50–65%) at low conversions (<20%) can be achieved over a V_2O_5/SiO_2 catalyst (12) but, as in the oxidation of propane, the reactants were diluted to avoid carbon deposition, and selectivities decreased as conversion increased.

EXPERIMENTAL

Apparatus. The reactor and experimental apparatus have been described previously for synthesis gas production by direct oxidation of methane (15) and for oxidative dehydrogenation of ethane (2).

A Pt coated α-alumina monolith 10 mm long in an 18 mm inner diameter quartz tube is the reactor. The edge

TABLE 2

Reactions of *n*-Butane

			% C_4H_{10} in air	ΔT_{ad} (°C)	C_4H_{10}/O_2	$\Delta H°$ (kJ/mol)	K_{eq} 1200 K
[6]	$C_4H_{10} + \frac{13}{2}O_2 \rightarrow 4CO_2 + 5H_2O$	Complete combustion	3.1	2700	0.15	−2657	$>10^{38}$
[7]	$C_4H_{10} + 2O_2 \rightarrow 4CO + 5H_2$	Partial oxidation to syngas	9.5	1688	0.50	−568	$>10^{30}$
[8]	$C_4H_{10} + \frac{1}{2}O_2 \rightarrow C_4H_8 + H_2O$	Oxidative dehydrogenation	29.6	778	2.00	−116	3.5×10^9
[9]	$C_4H_{10} + \frac{1}{2}O_2 \rightarrow 2C_2H_4 + H_2O$	Oxidative cracking	29.6	80	2.00	−12	5.2×10^{11}
[10]	$C_4H_{10} \rightarrow C_4H_8 + H_2$	Dehydrogenation	—	—	—	+126	4.3×10^1
[11]	$C_4H_{10} \rightarrow C_3H_6 + CH_4$	Cracking	—	—	—	+70	1.7×10^4
[12]	$C_4H_{10} \rightarrow C_2H_6 + C_2H_4$	Cracking	—	—	—	+92	1.0×10^3

TABLE 3

Reactions Producing Solid Carbon

		$\Delta H°$ (kJ/mol)	K_{eq} 1200 K	K_{exp} 1200 K
[13] $C_3H_6 \rightarrow 3C_s + 3H_2$	Cracking	−20	2.9×10^9	1.9×10^{-3}
[14] $C_2H_4 \rightarrow 2C_s + 2H_2$	Cracking	−53	6.9×10^5	2.6×10^{-2}
[15] $2CO \rightarrow C_s + CO_2$	CO disproportionation (Boudouard)	−172	1.7×10^{-2}	9.1
[16] $CO + H_2 \rightarrow C_s + H_2O$	Reverse steam reforming of carbon	−131	2.5×10^{-2}	68

of the monolith is sealed with high temperature alumina–silica cloth which acts as a layer of insulation and prevents bypass of the reactants around the outer edge of the catalyst. The monolith is also sandwiched between two inert alumina extruded monoliths which act as radiation shields and reduce the heat loss axially. The reaction zone is also insulated externally to reduce the heat loss radially.

The Pt catalyst was prepared by impregnation of an α-Al_2O_3 foam monolith disk with a saturated solution of H_2PtCl_6 in water as discussed elsewhere (2). The monolith used in this study had 45 pores per linear inch (ppi). The impregnated monolith was dried in N_2, calcined in air, and reduced in H_2. This process resulted in a loading of 5.1 wt% Pt for a single impregnation step and appeared to produce a uniform film of Pt metal ~0.5 μm thick which covered the alumina surface. After reaction, large Pt particles grew and bare alumina was exposed (15), although these changes appeared to be uncorrelated with reaction properties. In similar experiments over a 0.5 wt% Pt catalyst, the conversion and selectivity were essentially identical to the 5 wt% loading.

Gas flow rates into the reactor were controlled by mass flow controllers which had an accuracy of ±0.1 SLPM for all gases. The feed flow rates ranged from 1 to 9 SLPM total flow. These flow rates correspond to catalysts contact times (τ) from 3 to 25 milliseconds, upstream velocities (u_0) of 40 to 360 cm/sec, and flows of 1000 to 15,000 mol/hr. The product gases were fed through heated stainless steel lines to an automated gas chromatograph for quantitative analysis (2, 15). Individual species concentrations were measured with a reproducibility of ±2%. Some minor products (<2.5% selectivity) including C_2H_6, C_3H_8, and C_4H_{10} are not shown. It is important to note that oxygenates, C_2H_2, and any higher molecular weight hydrocarbons have selectivities of <0.1%.

TABLE 4

Product Distribution in *n*-Butane Conversion on a Carbon Atom Basis

	Pyrolysis	Oxidative dehydrogenation
Conversion	40	90
CH_4	18	10
C_2H_6	10	1
C_2H_4	20	35
C_3H_6	50	20
C_2H_2, C_4H_6, BTX	2	<0.1
CO	<0.2	20
CO_2	<0.2	10

The selectivity data shown was calculated on a carbon atom or a hydrogen atom basis. Carbon atom selectivities are calculated as a ratio of the moles of a specific product to the total moles of all products where these molar quantities have been scaled by the number of carbon atoms in the species, with corresponding balances for hydrogen atoms. This method of calculating the selectivity implicitly accounts for the mole number change due to reaction.

Temperature measurement. The reaction temperature was measured using a Pt–Pt/13% Rh thermocouple inserted from the rear of the reactor and located at the axis of the reactor tube between the catalytic monolith and the rear radiation shield. The steady state temperature at which the reactor operates is a function of the heat generated by the exothermic reactions, the heat consumed by the endothermic reactions, and the heat losses from the reactor. The calculated adiabatic reaction temperature, based on heats of reaction and the heat capacities of the reactants and products, was within 50°C of the measured reaction temperature, suggesting that the heat loss is negligible and the reactor is therefore nearly adiabatic.

Adiabatic temperature rises, ΔT_{ad}, for several individual reactions are listed in Tables 1 and 2. A simplified energy balance for the adiabatic reactor can be represented by

$$\overline{C}_p(\overline{T}_c - T_o) = \sum_i (-\Delta H_i)\overline{X}_i, \qquad [17]$$

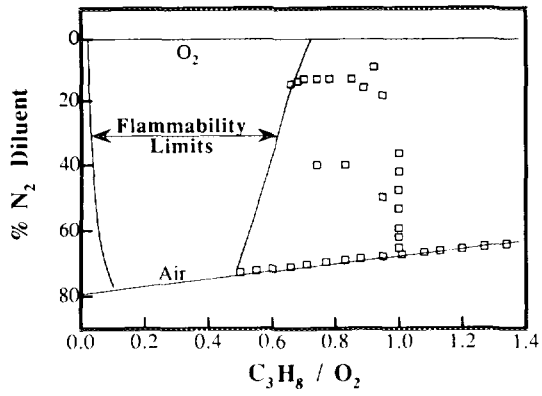

FIG. 1. Flammability limits of mixtures of propane and oxygen as a function of the N_2 dilution. Both upper and lower flammability limits are indicated for a range of compositions between propane in air and propane in oxygen (16). The boxes at the right indicate the compositions at which experimental data points exist.

where the bars over the quantities represent averages. In this expression, $\overline{C}_p(\overline{T}_c - T_o)$ is the sensible temperature rise of the catalyst surface from some gas temperature, T_o, to the average catalyst temperature, $\overline{T}_c$. The right hand side is the sum of the heats of reaction of both exothermic and endothermic reactions for some average conversion, $\overline{X}_i$, for each reaction.

Ignition. In order to initiate the reactions, a mixture of fuel and air near the stoichiometric composition for production of synthesis gas was fed to the reactor at a low flow rate (2 SLPM). The reactants were then preheated to the heterogeneous ignition temperature (200–250°C). After light-off, the preheating was turned off or set at the desired level and the other reaction parameters were adjusted to the desired conditions. After ~10 min, a steady state was established and product analysis began. All of the data shown were reproducible for time periods of several days.

Flames and explosions. It is important to note that mixtures of hydrocarbons and air or oxygen are flammable and will explode within some composition limits (16). For example, the flammability limits of mixtures of propane and air and/or oxygen are shown in Fig. 1 along with experimental data points in these experiments. Mixtures of propane and air are flammable between C_3H_8/O_2 ratios of 0.10 and 0.49, and as the amount of nitrogen diluent decreases, the flammability limits widen. Mixtures of propane and oxygen are flammable between C_3H_8/O_2 ratios of 0.02 and 0.72. Care must be taken to remain outside the flammability limits. To avoid flames and the possibility of explosions, experiments were always conducted in the fuel-rich regime at fuel/O_2 ratios greater than the upper flammability limit. Since this is a flow system, it is possible to operate within the flammability limits as long as the gas velocity exceeds the homogeneous flame speed.

RESULTS

We examined these reactions over many types of monoliths with different metals and loadings. While results varied slightly with loading, all results on the Pt catalyst were consistent with those shown below. Therefore, for clarity all of the results described below for the Pt catalyst will be for *a single catalyst* consisting of 5.1 wt% Pt on a 45 ppi foam alumina monolith. We describe variations with composition, N_2 diluent, flow rate, and preheating. We also report briefly on the selectivity of propane oxidation over Rh and Pd.

Propane

Air oxidation. Figure 2 shows the carbon atom and hydrogen atom selectivities and the propane conversion for the oxidation of propane in air over the 5.1 wt% Pt catalyst as a function of the C_3H_8/O_2 ratio in the feed. In these experiments, the relative amounts of propane and air were varied while maintaining a fixed total flow of 5 SLPM with room temperature feed.

As indicated in Table 1, below a C_3H_8/O_2 ratio of 0.5, we expect the products to be primarily CO_2 and H_2O from the complete combustion reaction (Eq. [1]) with the reaction temperature near 2800°C. As shown in Fig. 1, these compositions lay within the flammability limits, so experiments in this composition region were not performed because of overheating and the danger of explosion. Between C_3H_8/O_2 ratios of 0.5 and 0.7, production should switch from CO_2 and H_2O to CO and H_2 (Eq. [2]), the partial oxidation products, and the reaction temperature should decrease to ~900°C. As seen in Fig. 2, for C_3H_8/O_2 ratios less than 0.7, CO and H_2 are the dominant products.

At the stoichiometric composition for the production of synthesis gas (C_3H_8/O_2 = 0.67) we observe 30% *selectivity* to ethylene. In fact, at C_3H_8/O_2 ratios ≥0.67, ethylene and propylene are the dominant products. Ethylene selectivity peaks at ~30% at the synthesis gas stoichiometry with propane conversion >95% and propylene selectivity peaks at ~30% near a C_3H_8/O_2 ratio of 1.2 with a propane conversion of ~65%. At C_3H_8/O_2 ratios >0.8, the total olefin production (C_2H_4, C_3H_6, and C_4H_8) remains fairly constant with a selectivity of 55–60%. This selectivity peaks near a C_3H_8/O_2 ratio of 1.0. This is surprising since thermodynamics predicts the production of only CO, H_2, and graphite in this composition and temperature region. Figure 2 also shows that the ratio of the ethylene selectivity to the methane selectivity is nearly 2 : 1 on a carbon atom basis. This corresponds to one

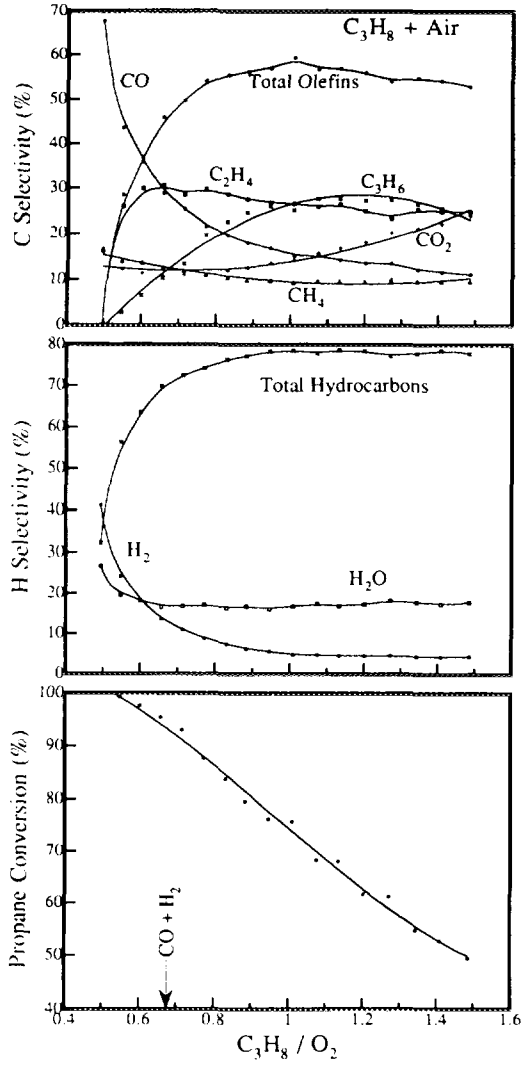

FIG. 2. Carbon selectivity, hydrogen selectivity, and propane conversion for a 45 ppi × 1 cm, 5.1 wt% Pt foam monolith as a function of C_3H_8/O_2 ratio in the feed at a total feed flow rate of 5 SLPM in an autothermal reactor at a pressure of 1.4 atm.

mole of ethylene formed for every mole of methane and supports the unimolecular cracking reaction (Eq. [5]).

Oxygen enrichment. As shown in Fig. 2, the optimum olefin yield in air is obtained near a C_3H_8/O_2 ratio of 1.0. Experiments were conducted at this C_3H_8/O_2 ratio to examine the effect of N_2 dilution. As shown in Fig. 3, the N_2 diluent was decreased from the air composition (62% N_2 at a C_3H_8/O_2 ratio of 1.0) to 36% N_2 diluent (a 1 : 1 N_2 : O_2 ratio). The level of N_2 dilution was not reduced beyond this point because the reaction temperature increased rapidly with decrease in dilution. Throughout this process, the total flow rate was maintained at 5 SLPM. Figure 3 shows the carbon atom and hydrogen atom selectivities, the propane conversion, and the reaction temperature as the level of dilution decreases.

Figure 3 shows the large effect of the diluent. This occurs primarily because the reaction is autothermal, and reduction in N_2 increases the reaction temperature from 940°C in air to 1010°C in the most O_2 enriched case. At the higher temperature, the propane conversion increases very quickly to 100%. Also, the selectivity to ethylene increases to >40% at complete propane conversion and the selectivity to propylene falls. Although ethylene selectivity improves at the higher temperature associated with the oxygen-enriched case, total olefin production is slightly higher at the lower temperatures.

Preheating. In Fig. 4, we show the effect of reactant preheating on selectivities, conversion, and reaction tem-

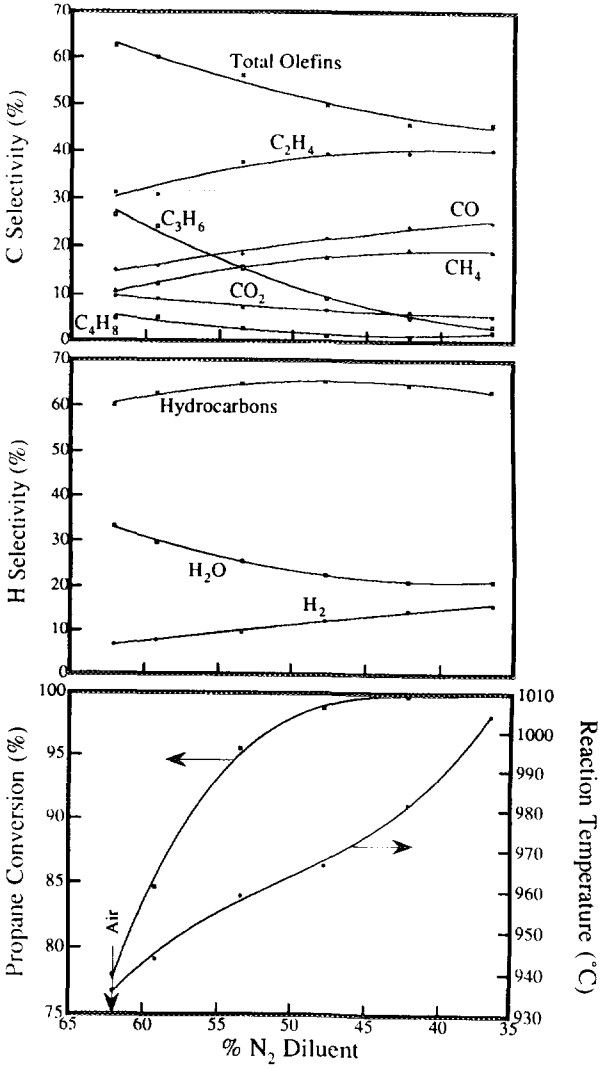

FIG. 3. Carbon selectivity, hydrogen selectivity, propane conversion, and reaction temperature for an 45 ppi × 1 cm, 5.1 wt% Pt foam monolith as a function of % N_2 diluent in the feed at a total flow rate of 5 SLPM and at a C_3H_8/O_2 ratio of 1.0 in an autothermal reactor at a pressure of 1.4 atm.

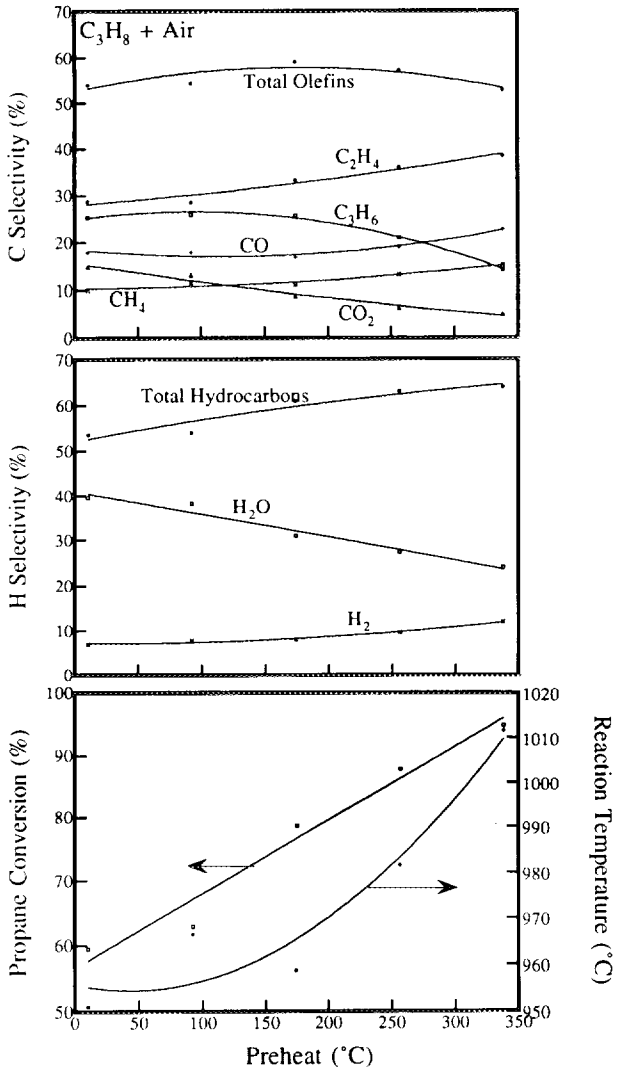

FIG. 4. Carbon selectivity, hydrogen selectivity, propane conversion, and reaction temperature for a 45 ppi × 1 cm, 5.1 wt% Pt foam monolith as a function of preheat temperature. The total flow rate was maintained at 5 SLPM. The C_3H_8/O_2 ratio was 1.0 at a pressure of 1.4 atm.

perature. The reactants are propane and air with a C_3H_8/O_2 ratio of 1.0 at a total flow rate of 5 SLPM. As shown in Fig. 4, preheating has similar effects to the reduction of nitrogen dilution (Fig. 3). The reaction temperature increased to 1010°C, which drove the propane conversion to >90%. Simultaneously, the ethylene selectivity improved at higher temperatures while the propylene selectivity fell. The total olefin production remained fairly constant between 55 and 60% selectivity.

Flow rate. Figure 5 illustrates the effect of varying the total flow rate on the selectivities and propane conversion for $C_3H_8:O_2:N_2$ ratio of 1 : 1 : 2. This corresponds to 50% N_2 dilution at a C_3H_8/O_2 ratio of 1.0. At increased flow rates, the propane conversion drops from nearly 100% at 1 SLPM to 75% at 9 SLPM and the ethylene selectivity drops slightly from 38 to 33%. However, the propylene selectivity increases dramatically from 11 to 25% as flow rate increases.

Alternate catalysts. Similar experiments were conducted over several different catalysts. Figure 6 shows the carbon atom selectivity for propane oxidation in air as a function of composition over a Pt/10% Rh gauze, a 4.0 wt% Rh monolith, and a 0.5 wt% Pd monolith. The Pt/10% Rh gauze gave results similar to those achieved over the Pt monolith (Fig. 2). Because the gauze was only 1 mm thick, a significantly shorter contact time of <1 msec was realized. This suggests that only the first portion

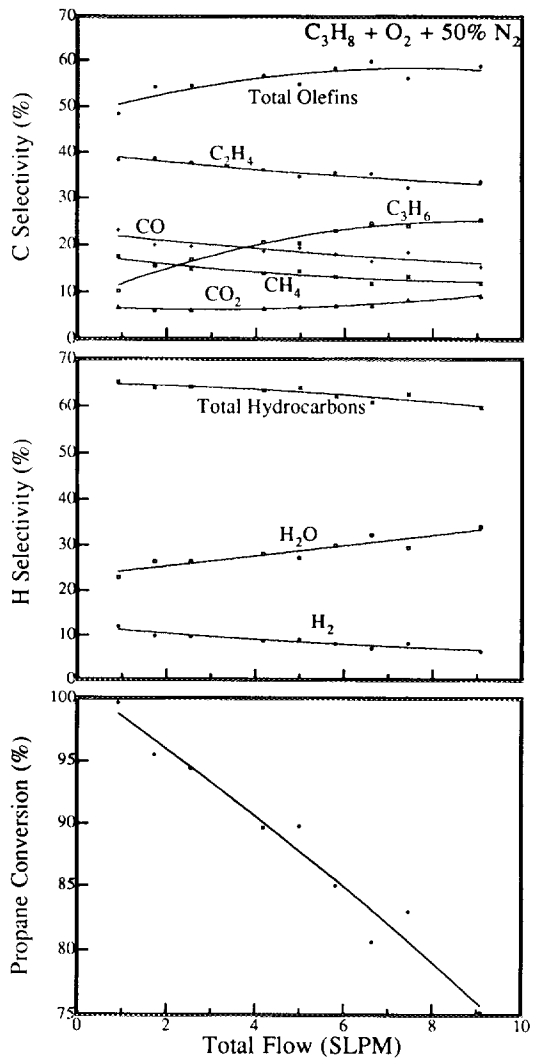

FIG. 5. Carbon selectivity, hydrogen selectivity, and propane conversion for a 45 ppi × 1 cm, 5.1 wt% Pt foam monolith as a function of reactant flow rate at a C_3H_8/O_2 ratio of 1.0 with 50% N_2 diluent in an autothermal reactor at a pressure of 1.4 atm.

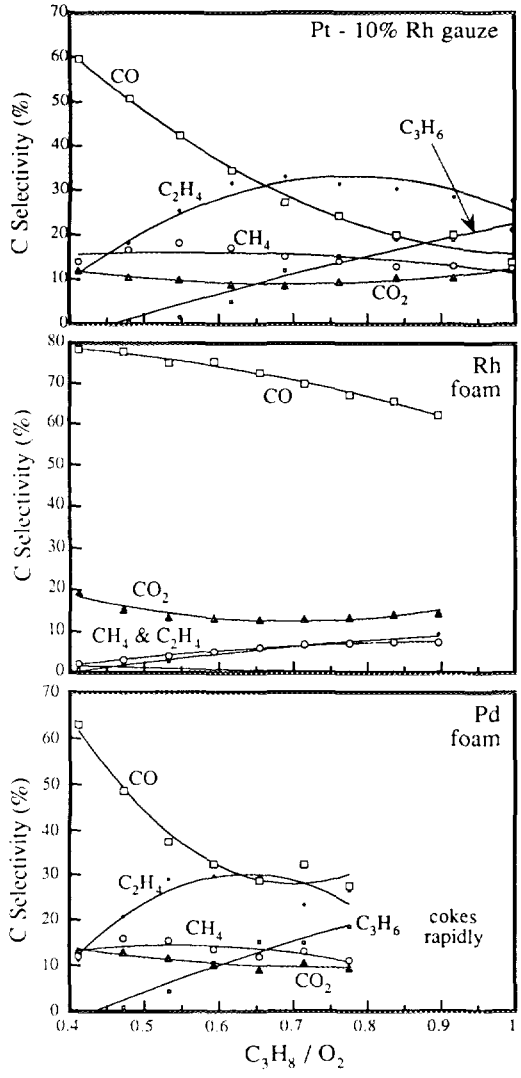

FIG. 6. Carbon selectivities obtained over 5 layers of Pt- 10% Rh gauze catalyst, a 4 wt% Rh foam monolith catalyst, and a 0.5 wt% Pd foam monolith catalyst as a function of feed composition at a total feed flow rate of 5 SLPM in an autothermal reactor at a pressure of 1.4 atm.

of the monolith is needed for the desired reactions. Unfortunately, the gauze lacked sufficient structural integrity and was brittle when removed from the reactor. The Rh monolith produced predominantly synthesis gas; there was no significant olefin production over the Rh catalyst. Although the Pd monolith initially showed excellent gas phase selectivities, it quickly deactivated and shut off within 15 min due to rapid carbon deposition.

n-Butane

Air oxidation. In Fig. 7, we show carbon and hydrogen atom selectivities, *n*-butane conversion, and the reaction temperature for the oxidation of *n*-butane in air over a 5.1 wt% Pt catalyst as a function of the C_4H_{10}/O_2 ratio. The relative amounts of *n*-butane and air were varied while maintaining a fixed total flow of 5 SLPM with room temperature feed.

As seen in Fig. 7, for C_4H_{10}/O_2 ratios less than 0.5, CO and H_2 are the dominant products. The reaction temperature is much less than 1600°C since the CO selectivity is much less than 100%. At C_4H_{10}/O_2 ratios $\geq$0.5, olefins are the dominant products which agrees with the expected products listed in Table 2. Ethylene selectivity peaks at ~32% at a C_4H_{10}/O_2 ratio of 0.65 with an *n*-butane conversion >90% and propylene selectivity increases at the higher C_4H_{10}/O_2 ratios reaching ~40% near a C_4H_{10}/O_2 ratio of 0.85 with a *n*-butane conversion of ~72%. Ther-

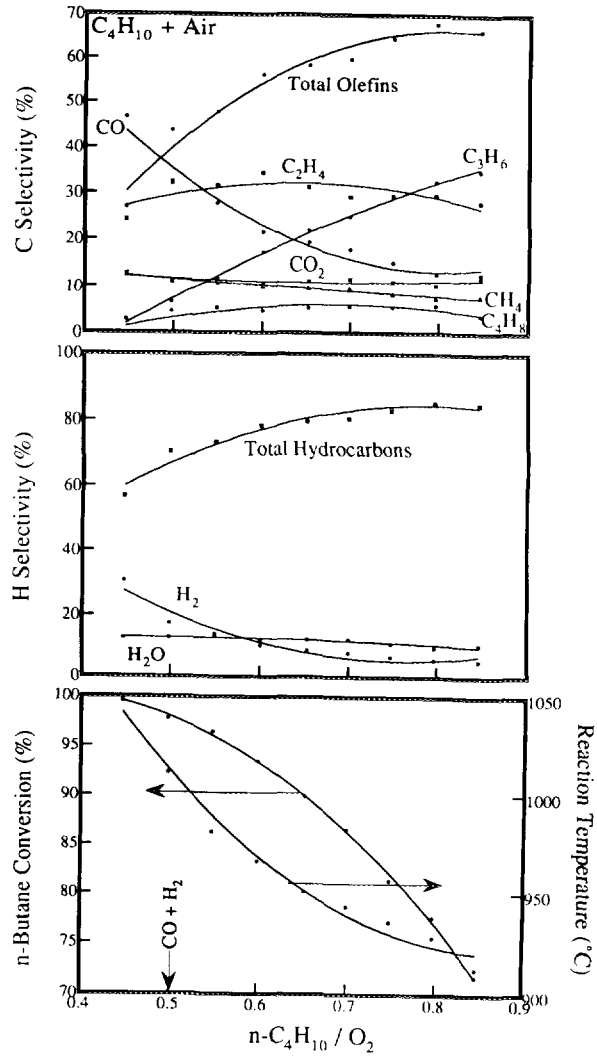

FIG. 7. Carbon selectivity, hydrogen selectivity, *n*-butane conversion, and reaction temperature for a 45 ppi × 1 cm, 5.1 wt% Pt foam monolith as a function of C_4H_{10}/O_2 ratio in the feed at a total feed flow rate of 5 SLPM in an autothermal reactor at a pressure of 1.4 atm.

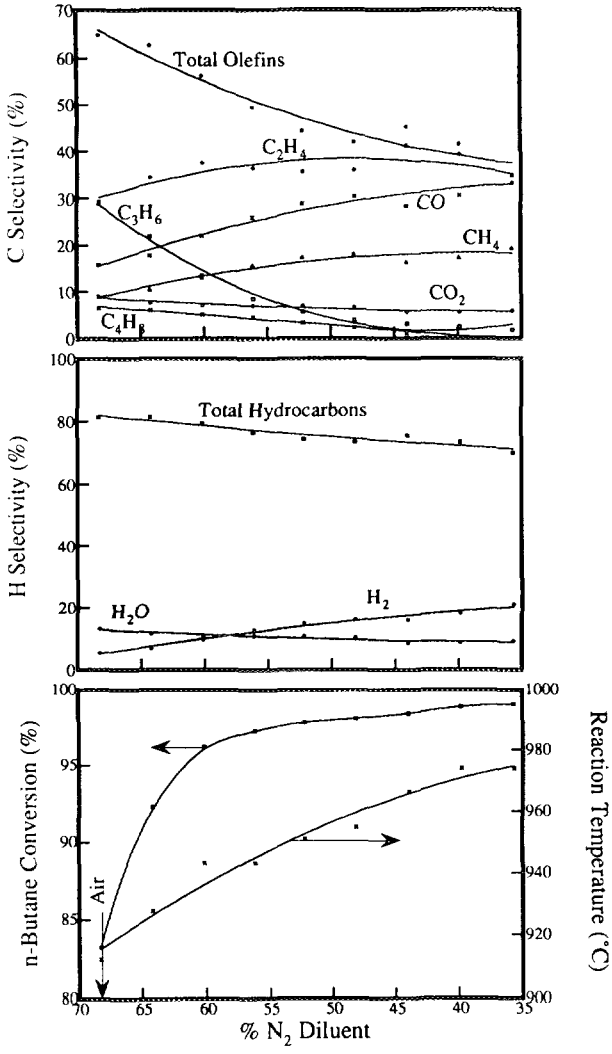

FIG. 8. Carbon selectivity, hydrogen selectivity, *n*-butane conversion, and reaction temperature for an 45 ppi × 1 cm, 5.1 wt% Pt foam monolith as a function of % N_2 diluent in the feed at a total flow rate of 5 SLPM and a C_4H_{10}/O_2 ratio of 0.7 in an autothermal reactor at a pressure of 1.4 atm.

modynamics predicts the production of only CO, H_2, and graphite in this composition and temperature region. Total olefin selectivity increases as the C_4H_{10}/O_2 ratio increases and reaches a plateau at ~65% selectivity.

Oxygen enrichment. As shown in Fig. 7, the optimum olefin selectivity is obtained at C_4H_{10}/O_2 ratios ≥0.7. Since the conversion decreases as the C_4H_{10}/O_2 ratio increases, the *optimum olefin yield* is obtained near a C_4H_{10}/O_2 ratio of 0.7. Experiments were conducted at this C_4H_{10}/O_2 ratio to determine the effect of the N_2 diluent. As shown in Fig. 8, the N_2 diluent was decreased from the air composition (68% N_2 at a C_4H_{10}/O_2 ratio of 0.7) to 35% N_2 diluent (a 1 : 1 N_2 : O_2 ratio). The total flow rate was maintained at 5 SLPM. Figure 8 shows the carbon and hydrogen atom selectivities, the *n*-butane conversion, and the reaction temperature as a function of the N_2 dilution.

Reduction in N_2 increases the reaction temperature from 920°C in air to 970°C, and the *n*-butane conversion increases rapidly and approaches 100%. At these higher temperatures, the selectivity to ethylene increases slightly to ~40% at an *n*-butane conversion of ~98%, and the selectivity to propylene falls to nearly zero. The total olefin production decreases steadily as the N_2 dilution decreases.

Figure 9 illustrates the variation in selectivities and conversion with the C_4H_{10}/O_2 ratio at a fixed level of 50%

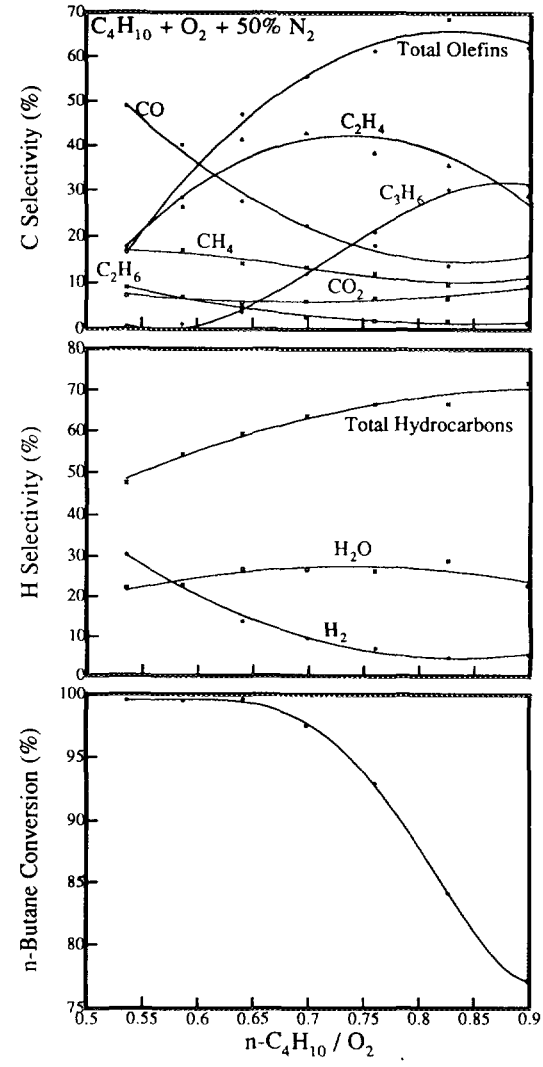

FIG. 9. Carbon selectivity, hydrogen selectivity, and *n*-butane conversion for a 45 ppi × 1 cm, 5.1 wt% Pt foam monolith as a function of C_4H_{10}/O_2 ratio in the feed with 50% N_2 diluent at a total feed flow rate of 5 SLPM in an autothermal reactor at a pressure of 1.4 atm.

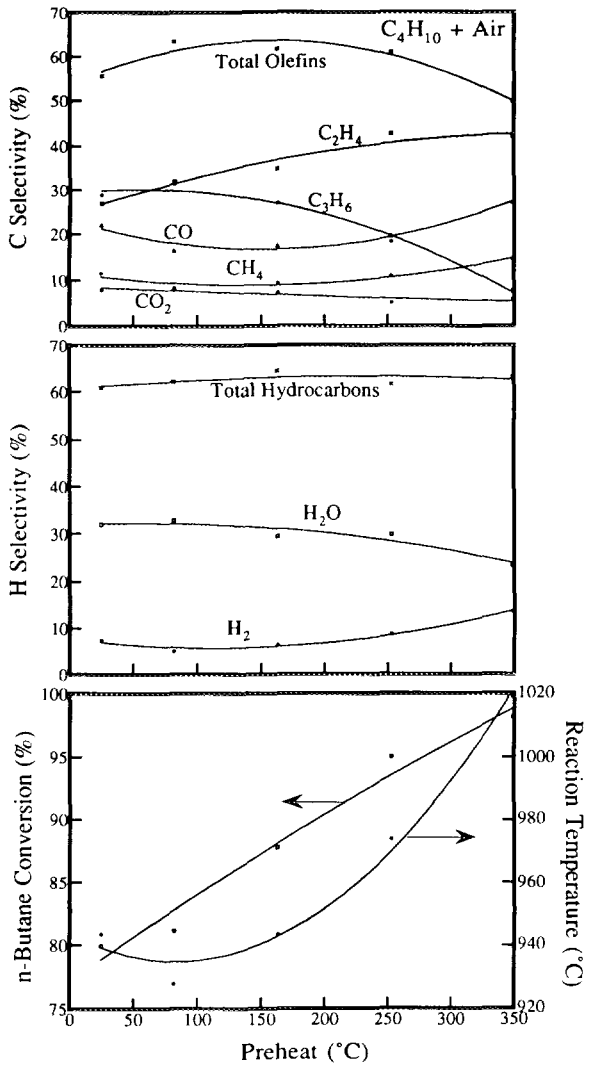

FIG. 10. Carbon selectivity, hydrogen selectivity, *n*-butane conversion, and reaction temperature for a 45 ppi × 1 cm, 5.1 wt% Pt foam monolith as a function of preheat temperature. The total flow rate was maintained at 5 SLPM. The C_4H_{10}/O_2 ratio was 0.7 at a pressure of 1.4 atm.

N_2 dilution. Similarly to Fig. 7, ethylene selectivity peaks near a C_4H_{10}/O_2 ratio of 0.7, but now reaches >40% at >95% conversion of *n*-butane compared to 32% ethylene selectivity at 85% conversion for oxidation in air. Also, as observed in the air experiments, the propylene selectivity increases as the C_4H_{10}/O_2 ratio increases. However, the propylene selectivity is slightly lower in the oxygen-enriched experiments than it was in the air experiments.

Preheating. In Fig. 10, we show the effect of reactant preheating on the selectivities, conversion, and reaction temperature. In this case, we return to *n*-butane oxidation in air, again with a C_4H_{10}/O_2 ratio of 0.7 at a total flow rate of 5 SLPM. Prehating has similar effects to the reduction of nitrogen dilution (Fig. 8). The reaction temperature increased to 1020°C which drove the *n*-butane conversion to >95%. Simultaneously, the ethylene selectivity improved at higher temperatures, exceeding 40% and the propylene selectivity rapidly fell. Higher temperatures favor ethylene production, but reduce propylene production.

Flow rate. Figure 11 illustrates the effect on the selectivities and *n*-butane conversion of varying the total flow rate. A C_4H_{10}/O_2 ratio of 0.7 was maintained throughout with an O_2 enriched air stream equivalent to 50% N_2 diluent. At higher flow rates, the *n*-butane conversion drops from 100 to 87% and the ethylene selectivity drops slightly from 44 to 38%, but the propylene selectivity increases

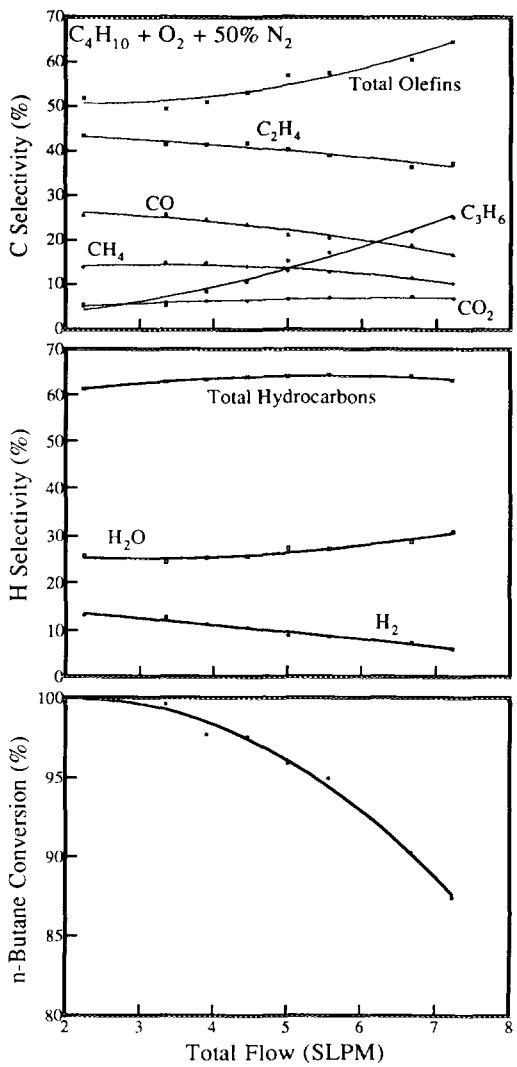

FIG. 11. Carbon selectivity, hydrogen selectivity, and *n*-butane conversion for a 45 ppi × 1 cm, 5.1 wt% Pt foam monolith as a function of reactant flow rate at a C_4H_{10}/O_2 ratio of 0.7 with 50% N_2 diluent in an autothermal reactor at a pressure of 1.4 atm.

dramatically from 5 to 28% at a flow rate of 7 SLPM. As a result, total olefin selectivity increases from 50 to 65% at the higher flow rates.

DISCUSSION

There are several surprising features of these experiments: (1) Olefins are produced from propane and *n*-butane *with up to 65% selectivity at nearly 100% fuel conversion* over a Pt loaded foam monolith. (2) Although thermodynamics predicts rapid carbon deposition, which would result in catalyst deactivation, no coke formation or deactivation is observed over the Pt catalyst for operation for many hours. (3) Propane and *n*-butane oxidations result in very similar product distributions and negligible butylene is formed in *n*-butane oxidation. (4) Under conditions where propane and *n*-butane are completely reacted (1000°C), ethylene and propylene survive.

In a previous paper (2) we discussed similar phenomena observed in the oxidative dehydrogenation of ethane. In the following sections, we will expand upon the mechanism proposed for ethane (2) to include propane and *n*-butane oxidative dehydrogenation and cracking.

It is important to emphasize that these experiments have been conducted in the severely fuel-rich regime. In both the propane and the *n*-butane experiments, the C_3H_8/O_2 or C_4H_{10}/O_2 ratios are typically five times the ratio required for complete combustion to CO_2 and H_2O. Oxygen is always the limiting reactant, and *oxygen is always completely consumed.* We did not approach the CO_2 and H_2O stoichiometry ($C_3H_8/O_2 = 0.33$, $C_4H_{10}/O_2 = 0.25$, see Fig. 1) because the system would overheat, become flammable, or explode.

A reaction mechanism must address several factors, including (1) the absence of carbon deposition under conditions where it is thermodynamically favorable, (2) the similarity of the product distributions for either propane or *n*-butane fuel, (3) ethylene production increases with temperature while propylene production decreases, and (4) propylene selectivity increases at higher flow rates. We suggest that these observations can be accounted for by the reaction steps shown in Figs. 12 and 13 for propane and *n*-butane oxidations, respectively.

Thermal Pyrolysis versus Catalytic Oxidation

As discussed previously for ethane (2), in either propane or *n*-butane oxidation a simple pyrolysis mechanism would not predict the observed high selectivities to propylene or ethylene. In homogeneous pyrolysis of propane and *n*-butane, acetylene, butadiene, and aromatic compounds are detected and account for as much as 15% of the product (3). None of these compounds is present in detectable amounts and, based on the product analysis, none can be present as more than 0.1% of the total products in any of the results shown. As shown in Table 4, the product selectivity distribution obtained in thermal pyrolysis of *n*-butane (10) does not agree with the product selectivity distribution observed here. We see 75% more C_2H_4, 10 times less CH_4, and 10 times less C_2H_6 compared to the pyrolysis experiments, even though our conversions are 90% versus 40% in pyrolysis.

We believe that all of the observed results can be accounted for by assuming only surface reactions with no significant homogeneous reactions or flames. Arguments against homogeneous reactions are (1) feed compositions outside the flammability regime, (2) very high flow velocity, (3) high surface area to scavenge radical chain propagators, (4) a large observed sensitivity to the nature of the catalyst surface, and (5) an absence of mixed and polymeric products.

Perhaps the strongest arguments against homogeneous reaction is the very short reaction time needed on the catalyst (<5 msec) compared to the times needed in thermal pyrolysis reactors (0.1 to 1 sec) at comparable temperatures and pressures. At the much shorter times of the catalytic processes, much higher conversions of hydrocarbon reactants occur. In experiments to be published later, we have also conducted these reactions at pressures up to 5 atm without dilution and have seen no significant change in product distribution or increase in carbon formation. Homogeneous reaction products should change significantly with pressure.

However, there are considerable similarities in steps between purely homogeneous reactions and these experiments, because in both cases the reactant alkanes dissociate unimolecularly to form alkyl species which then react to form other intermediates and products. The adsorbed alkyl species on noble metal surfaces probably have similar structures to the gas phase alkyls as will be discussed later.

In thermal pyrolysis there are no barriers to complete cracking to C_1 species and coke, and higher conversion produces much more coke. Addition to H_2O does not appear to cause significant homogeneous steam reforming of the hydrocarbons because little CO or CO_2 are formed in spite of large excess of H_2O, but H_2O suppresses carbon, presumably by surface reaction of H_2O with C_s on the walls of the pyrolysis reactor. Most publications on pyrolysis note contributions from surface reactions on the tube walls in those experiments, but their role appears unclear (7, 11).

In our experiments the surface accomplishes several goals: (1) enhanced dissociation of alkanes by hydrogen abstraction with adsorbed oxygen, (2) the bonding of the adsorbed alkyl on the surface and efficient energy exchange for it to further decompose, and (3) the reduction of bimolecular reaction steps. The latter are especially interesting differences between homogeneous and hetero-

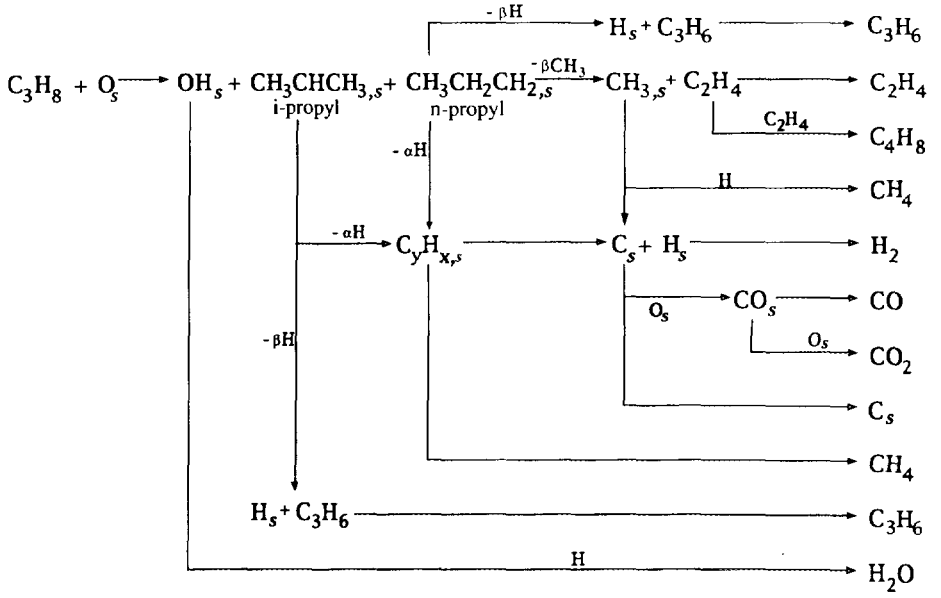

FIG. 12. Proposed surface reactions in propane oxidation. The gaseous species produced are indicated at the right.

geneous reaction processes. The adsorbed alkyls cannot easily react with gas molecules because their reactive ends are bound to the surface. Therefore, the efficient energy exchange at the surface allows unimolecular reactions of adsorbed alkyls such as β-H and β-alkyl elimination to dominate and yield the simple mix of products observed.

The only paths to bimolecular surface reactions probably require surface diffusion of alkyl species, and, since coverages of alkyls are low, these are not favored. Even surface reactions with H_S (which would form alkanes) are probably unimportant because, while adsorbed hydrogen atoms have very high surface mobilities on noble metals, the coverage of adsorbed H (E = 25 kcal/mol) is calculated to be ~0.01 monolayers at 1000°C with P_{H_2} = 10 Torr.

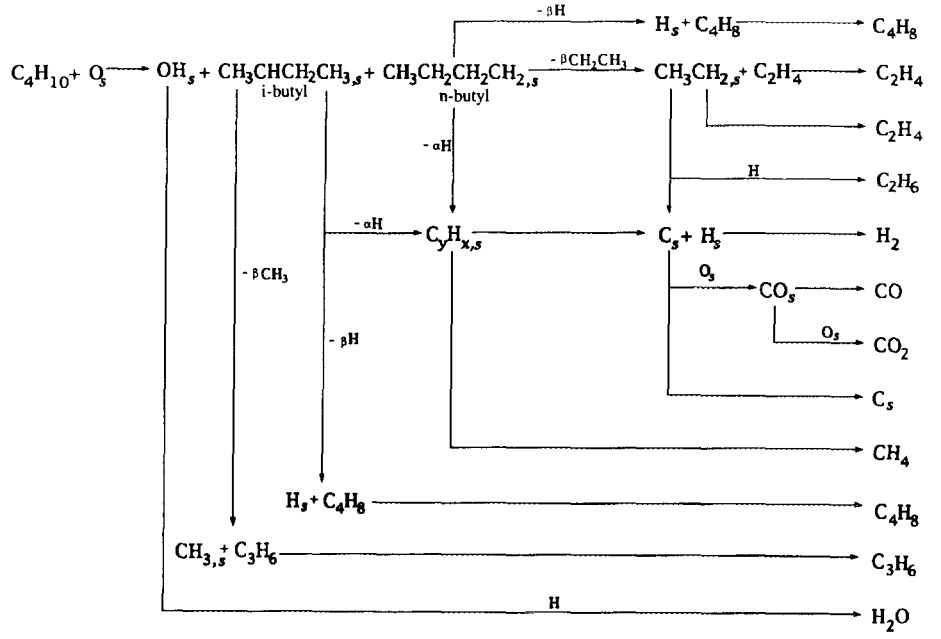

FIG. 13. Proposed surface reactions in n-butane oxidation. The gaseous species produced are indicated at the right.

Of course a major difference between these experiments and pyrolysis is the presence of oxygen. However, we note that O_2 is quickly converted completely to H_2O, CO, and CO_2 which are much less reactive, and our experiments in fact have less H_2O and a smaller fraction of total oxygen than do conventional steam cracking experiments.

Noble metals are highly effective alkane hydrogenolysis and cracking catalysts (17, 18) even at quite low temperatures. Therefore, the catalytic cracking of large alkanes to olefin plus smaller alkane is expected to be very efficient.

Reaction Steps

Both propane and butane oxidation can be simplified from the steps shown in Figs. 12 and 13 to five essential steps,

$$\text{alkane} \xrightarrow{r_i} \begin{matrix}\text{surface}\\ \text{alkyl}\end{matrix} \xrightarrow{r_\beta} \text{olefin} \xrightarrow{r_{crack}} \begin{matrix}\text{smaller}\\ \text{olefin}\end{matrix} \xrightarrow{r_\alpha} C_S \xrightarrow{r_{CO}} CO, \quad [18]$$

where olefins are formed by both β-hydrogen and β-alkyl elimination.

Initiation. We suggest that the most probable initiation step's the abstraction of hydrogen from the alkane by adsorbed oxygen atoms, O_S,

$$C_3H_8 + O_s \rightarrow C_3H_{7,s} + OH_s \quad [19]$$

$$C_4H_{10} + O_s \rightarrow C_4H_{9,s} + OH_s, \quad [20]$$

to form a surface alkyl group. This initiation step is plausible since the front region of the Pt catalyst should be completely covered by O_S. The kinetics of oxygen interactions with a Pt surface are well understood (19). Assuming dissociative adsorption, $s \approx 0.01$, and $E_a = 52$ kcal/mol, a Langmuir isotherm predicts $\theta_o \approx 0.99$ monolayers of O_S under reaction conditions (900°C, $P_{O_2} \approx 170$ Torr) at the front face of the catalyst before any reactions take place. The alkane entering the catalytic monolith should therefore always find O_S for reaction 19 or 20 rather than a clean surface for reactions 4–5 and 10–12.

Since the reactions are carried out in the fuel rich regime and thus are oxygen limited, gaseous O_2 is quickly consumed so that the O_S is completely depleted at some distance into the catalytic monolith and the remainder of the catalyst surface is likely covered with a fraction of a monolayer of carbon. From experiments with gauzes less than 1 mm thick and with thinner ceramic foam monoliths, we estimate that this occurs in less than 1 mm of the catalyst, which corresponds to a contact time of ~500 μsec for the flow rates used here.

If this step is the rate limiting step and occurs in the first 10% of the monolith, then a first order pseudo-homogeneous rate constant, k_i, can be calculated for a τ of 0.5 milliseconds and 95% conversion to be 6000 sec^{-1}.

β-Hydrogen and alkyl elimination. Once adsorbed on the Pt surface, the alkyl groups may undergo a variety of decomposition reactions. Both the propyl and butyl groups may be adsorbed at a primary carbon atom or at a secondary carbon. Olefin formation *cannot occur* from any of these adsorbed species by either α-hydrogen elimination or α-alkyl elimination. As shown in Eq. [18], these mechanisms would lead to the complete decomposition of the alkyl to C_S and H_S, which may then form CO and H_2 or remain on the surface as coke. Both β-hydrogen and β-alkyl elimination, however, can lead to olefin production.

The interactions of alkyl groups on several catalyst surfaces, including Pt, have been examined (20, 21). The decomposition of the adsorbed alkyl groups has been characterized using temperature programmed desorption (TPD) and X-ray photoelectron spectroscopy (XPS) in an ultra-high vacuum (UHV) system (18, 21). The Pt surface was exposed to an alkyl halide (i.e., C_2H_5I) which decomposed to produce adsorbed alkyl groups. It was shown that the first hydrogen abstracted was primarily by β-elimination, resulting in ethylene formation. Similar work on a Cu(111) surface (22) postulates a surface transition state which preferentially leads to β-hydrogen and β-alkyl elimination.

A propyl group adsorbed at a 1° carbon can undergo either β-hydrogen elimination to form propylene or β-alkyl elimination to form ethylene and adsorbed methyl,

$$CH_3CH_2CH_{2,s} \rightarrow CH_{3,s} + C_2H_4. \quad [21]$$

There is evidence that C–C bonds are weaker than C–H bonds (23) and based on the known kinetic data for gas phase radical reactions, ethylene should be formed three times more quickly than propylene (24). These rates should be similar for the adsorbed species and thus, the β-alkyl elimination reaction to form ethylene is preferred. A propyl group adsorbed at a 2° carbon cannot eliminate a β-alkyl and therefore can undergo only β-hydrogen elimination to form propylene:

$$CH_3CHCH_{3,s} \rightarrow H_s + C_3H_6. \quad [22]$$

Likewise, a butyl group adsorbed at a 1° carbon can undergo either β-hydrogen elimination to form butylene or β-alkyl elimination to form ethylene:

$$CH_3CH_2CH_2CH_{2,s} \rightarrow C_2H_{5,s} + C_2H_4. \quad [23]$$

Ethylene formation is preferred in this case since the C–C

bond is more vulnerable than the C–H bond (23). A butyl group adsorbed at a 2° carbon can undergo either β-hydrogen elimination to form butylene or β-alkyl elimination to form propylene:

$$CH_3CHCH_2CH_{3,s} \rightarrow CH_{3,s} + C_3H_6. \quad [24]$$

Similarly, propylene formation is preferred due to the preference for β-alkyl elimination over β-hydrogen elimination reactions (23). This explains the lack of butylene as a major reaction product.

On Rh and Pd catalysts, α-elimination reactions also occur. On either Pt or Pd, 50–70% of the surface alkyl reacts through the β channel, resulting in olefin production ($r_\beta/(r_\alpha + r_\beta) = 0.5$ to 0.7). On Rh, a more reactive surface than either Pt or Pd, only 10% goes to olefins ($r_\beta/(r_\alpha + r_\beta) = 0.1$).

Sequential reactions. Our proposed surface reaction steps are shown in Figs. 12 and 13 for propane and *n*-butane oxidation, respectively. These diagrams list only a few of the possible secondary reactions. For example, Fig. 12 lists the dimerization of ethylene to form butylene as a major route to ethylene production loss, but not steam reforming or thermal cracking reactions. In fact, these secondary reactions are probably the dominant routes to propylene loss.

After propylene is formed, either by β-hydrogen elimination from propane or by β-alkyl elimination from butane, it is vulnerable to secondary reactions. Since a significant amount of water is present (~30% selectivity), propylene can react by steam reforming:

$$C_3H_6 + 3H_2O \rightarrow 3CO + 6H_2. \quad [25]$$

Also, propylene can undergo thermal cracking to form ethylene:

$$C_3H_6 \rightarrow C_2H_4 + CH_{2,s}. \quad [26]$$

This leaves a methylene species on the surface which can either be further dehydrogenated, leading to coking, or react with surface hydrogen and desorb as CH_4 or with surface oxygen to desorb as CO. These sequential reactions affect the observed selectivity distributions and their contributions are presumably controlled by the catalyst contact time.

The mechanism also explains the increase in propylene selectivity at high flow rates shown in Figs. 5 and 11. At higher flow rates (shorter contact times), the product propylene spends less time in the reaction zone, so less propylene is lost to thermal cracking (Eqs. [13] or [25]). The other product selectivities remain relatively constant, suggesting that ethylene is a primary reaction product and is not lost in subsequent reactions.

At higher reaction temperatures (obtained either by preheat or by the reduction of N_2 diluent) the product selectivities change. As shown in Fig. 8 for *n*-butane oxidation, as the temperature increases, the propylene selectivity decreases and the methane selectivity increases. At higher temperatures, thermal cracking reactions increase, thus increasing the ethylene yield as product propylene is lost to thermal cracking (Eqs. [13] or [26]). Propylene loss is accompanied by an increase in methane.

As in Eq. [18], some atomic carbon is adsorbed on the surface. On either Pt or Pd, 30–50% of the reactant alkane passes through a C_S intermediate ($r_\beta/(r_\alpha + r_\beta) = 0.5$ to 0.7); on Rh, 90% goes through C_S ($r_\beta/(r_\alpha + r_\beta) = 0.1$). However, on either Pt or Rh, all of the C_S leaves the surface as CO or CO_2 ($r_{CO} = r_\alpha$). This is not the case on Pd where enough C_S remains on the surface to rapidly deactivate the catalyst ($r_{CO} < r_\alpha$).

Relative rate constants. By examining the relative production of propylene compared to the production of ethylene as a function of reaction temperature for propane oxidation (Fig. 4), we can extract relative rates. To do this, we assume that there are only two competing reactions, namely, the β-hydrogen elimination reaction producing propylene and the β-alkyl elimination reaction producing ethylene. We also assume that these steps do not involve oxygen. The validity of these assumptions will be discussed below.

The propane system can then be reduced to

$$C_3H_8 \xrightarrow{r_{\beta H}} C_3H_6 + H_2, \quad r_{\beta H} = k_{\beta H}[C_3H_8] \quad [27]$$

$$C_3H_8 \xrightarrow{r_{\beta R}} C_2H_4 + CH_4, \quad r_{\beta R} = k_{\beta R}[C_3H_8]. \quad [28]$$

We can relate the rates of these reactions by the ratio of the partial pressures of their products.

$$\frac{P_{C3H6}}{P_{C2H4}} = \frac{r_{\beta H}}{r_{\beta R}} = \frac{k_{\beta H_0}}{k_{\beta R_0}} \exp\left[\frac{-(E_{A\beta H} - E_{A\beta R})}{RT}\right], \quad [29]$$

where P_i is the partial pressure of species i produced per mole of fuel and r_i is the rate of formation of species i and Fig. 14 shows an Arrhenius relationship for these ratios.

From this relationship, we can estimate relative preexponentials and activation energy differences. The activation energy for hydrogen elimination is 46 kcal/mol K less than the activation energy for β-alkyl elimination. This suggests that the β-alkyl elimination reactions favor higher temperatures which agrees with the observation of increased ethylene production at higher temperatures. In the *n*-butane system, the activation energy for β-methyl

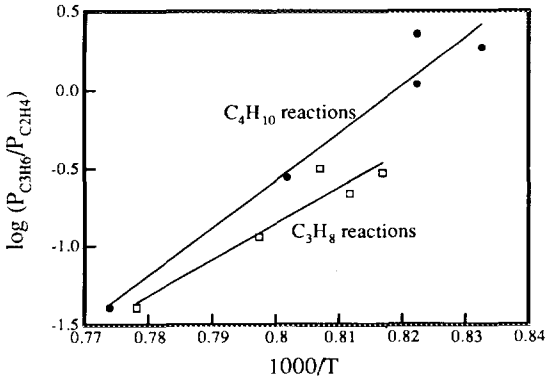

FIG. 14. Comparison of the rate of formation of propylene relative to the rate of formation of ethylene for propane and *n*-butane oxidation.

elimination is 61 kcal/mol K less than the activation energy for β-ethyl elimination.

For both the propane and *n*-butane systems, these values do not describe elementary reaction steps, but rather a lumping of several contributing parameters. If the simplification discussed in this section was sufficient to capture the true characteristics of these systems, then the ratios of the preexponentials should have been nearly 1. The fact that these values are instead 3×10^{-9} and 1×10^{-11} for propane and *n*-butane, respectively, indicates that mass transfer to the surface and the surface coverages of the various forms of the alkyls play significant roles in the resulting product distributions.

Equilibrium

Similar to the oxidative dehydrogenation ethane to ethylene (2), these experiments were conducted under conditions where thermodynamics predicts carbon deposition (graphite) at all fuel/O_2 ratios greater than that for synthesis gas formation. These equilibrium calculations were conducted using a packaged program that minimizes the free energy for a given set of reactants and possible products at a given temperature and pressure. The program considers only thermodynamic equilibrium and does not allow for catalytic interactions. The allowed products in these calculations were C_1–C_4 paraffins and olefins, acetylene, CO, CO_2, C_S (graphite), H_2, H_2O, O_2, and N_2 (inert).

Equilibrium for a feed with a C_3H_8 : O_2 ratio of 1 predicts that 30% of the carbon should remain on the surface as graphite. At the flow rates of these experiments, if even a small fraction of this graphite was actually forming, then the catalyst would deactivate in minutes. This is the apparent cause of the deactivation of the Pd catalyst. Since no carbon deposition is observed over the Pt catalyst and no deactivation occurs over several hours of operation, these cannot be equilibrium reactions, and the Pt surface must be exposed.

There are at least four primary routes to the production of C_S including olefin cracking (Eqs. [13] and [14]), the Boudouard reaction (Eq. [15]) and reverse steam reforming (Eq. [16]). These reactions are listed in Table 3 with their equilibrium constants and experimental values, K_{exp}, of the equilibrium constants (ratios of partial pressures) obtained under reaction conditions for propane oxidation in O_2 (20% N_2 diluent) over a 5.1 wt% Pt catalyst at a fuel/O_2 ratio of 1.

$$K_{C_3H_6} = \frac{P_{H_2}^3 a_c}{P_{C_3H_6}} \quad [30]$$

$$K_{C_2H_4} = \frac{P_{H_2}^2 a_c}{P_{C_2H_4}} \quad [31]$$

$$K_{CO} = \frac{P_{CO_2} a_c}{P_{CO}^2} \quad [32]$$

$$K_{H_2O} = \frac{P_{H_2O} a_c}{P_{CO} P_{H_2}}, \quad [33]$$

where P_i are partial pressures and a_c is the activity of solid carbon. The values for K_{exp} (Eqs. [30]–[33]) in Table 3 were obtained assuming $a_c = 1$, for equilibrium in solid graphite formation.

Since K_{eq} is many orders of magnitude greater than K_{exp} for the olefin cracking reactions (Eqs. [13] and [14]), these reactions cannot attain equilibrium if the catalyst does not deactivate. For the Boudouard reaction (Eq. [15]) and reverse steam reforming (Eq. [16]), however, $K_{eq} < K_{exp}$ suggesting that the reverse of these reactions takes place.

In summary, although carbon may be deposited on the surface by hydrocarbon cracking, in these experiments, the CO_2 and H_2O partial pressures are sufficiently high to completely suppress this coking and continuously remove any coke from the surface by either CO_2 reforming or steam reforming.

CONCLUSIONS

Ethylene and propylene are produced from ethane, propane, or *n*-butane at high conversions of hydrocarbon and total conversion of oxygen at atmospheric pressure over Pt-coated monoliths with residence times on the order of milliseconds. The role of oxygen in these reactions appears to be that of an initiator in forming the surface alkyl group by abstraction of a hydrogen atom from the alkane by surface oxygen, O_S. On Pt, the surface alkyl then undergoes β-hydrogen elimination or β-alkyl elimination to form ethylene and propylene. On Rh or Pd, it undergoes α-hydrogen or α-alkyl elimination to form C_S and perhaps CO.

The short contact times and the presence of H_2O and CO_2 appear to completely suppress surface carbon formation to allow olefin formation at high conversion.

The formation of simple product distributions and the absence of small alkanes argues that these processes occur primarily on the surface. The strong dependence on the nature of the metal is further support for primarily heterogeneous reactions, and suggests that the proper choice of catalyst can be used to "tune" these oxidation processes for even higher yields of a desired product.

REFERENCES

1. Seshan, K., Swaan, H. M., Smits, R. H. H., van Omens, J. G., and Ross, J. R. H., *in* "New Developments in Selective Oxidation," (G. Centi and F. Trifiro, Eds.), pp. 505–512. Elsevier, Amsterdam, 1990.
2. Huff, M., and Schmidt, L. D., *J. Phys. Chem.* **97,** 11815 (1993).
3. McConnell, C. F., and Head, B. D., *in* "Pyrolysis: Theory and Industrial Practice," (L. F. Albright, B. L. Crynes and W. H. Corcoran, Eds.), pp. 25–45. Academic Press, New York, 1983.
4. Sundaram, K. M., and Froment, G. F., *Ind. Eng. Chem. Fundam.* **17,** 174 (1978).
5. Nguyen, K. T., and Kung, H. H., *J. Catal.* **122,** 415 (1990); Chaar, M. A., Patel, D., and Kung, H. H., *J. Catal.* **109,** 463 (1988).
6. Smits, R. H. H., Seshan, K., and Ross, J. R. H., *J. Chem. Soc., Chem. Commun.* 558 (1991).
7. Burch, R., and Crabb, E. M., *Appl. Catal. A* **100,** 111 (1993).
8. Komatsu, T., Uragami, Y., and Otsuka, K., *Chem. Lett.* 1903 (1988).
9. Kung, M. C., and Kung, H. H., *J. Catal.* **134,** 668 (1992).
10. Corcoran, W. H., *in* "Pyrolysis: Theory and Industrial Practice," (L. F. Albright, B. L. Crynes, and W. H. Corcoran, Eds.) pp. 47–68. Academic Press, New York, 1983.
11. Delzer, G. A., and Kolts, J. H., *in* "Novel Production Methods for Ethylene, Light Hydrocarbons, and Aromatics," (L. F. Albright, B. L. Crynes, and S. Nowak, Eds.) pp. 41. Dekker, New York, 1992.
12. Owens, L., and Kung, H. H., *J. Catal.* **144,** 202 (1993); Patel, D., Andersen, P. J., and Kung, H. H., *J. Catal.* **125,** 132 (1990); Chaar, M. A., Patel, D., Kung, M. C., and Kung, H. H., *J. Catal.* **105,** 483 (1987).
13. Armendariz, H., Aguilar-Rios, G., Salas, P., Valenzuela, M. A., Schifter, I., Arriola, H., and Nava, N., *Appl. Catal. A* **92,** 29 (1992).
14. Heiman, J. C. *in* "Pyrolysis: Theory and Industrial Practice," (L. F. Albright, B. L. Crynes, and W. H. Corcoran, Eds.) pp. 365–375. Academic Press, New York, 1983.
15. Hickman, D. A., and Schmidt, L. D., *J. Catal.* **138,** 267 (1992); Hickman, D. A., Haupfear, E. A., and Schmidt, L. D., *Catal. Lett.* **17,** 223 (1993); Hickman, D. A., Huff, M., and Schmidt, L. D., *Ind. Eng. Chem. Res.* **32,** 809 (1993).
16. Lewis, B., and von Elbe, G., "Combustion, Flames and Explosions of Gases," Academic Press, New York, 1951.
17. Gao, S., and Schmidt, L. D., *J. Catal.* **115,** 356 (1989); *J. Catal.* **111,** 210 (1988).
18. Zaera, F., *Acc. Chem. Res.* **25,** 260 (1992).
19. Brundle, C. R., and Broughton, J. Q., *in* "The Chemical Physics of Solid Surfaces and Heterogeneous Catalysis," (D. A. King and D. P. Woodruff, Eds.) Vol. 3. Elsevier, Amsterdam, 1990.
20. Jenks, C. J., Chiang, C.-M., and Bent, B. E., *J. Am. Chem. Soc.* **113,** 6308 (1991).
21. Zaera, F., *Surf. Sci.* **219,** 453 (1989).
22. Forbes, J. G., and Gellman, A. J., *J. Am. Chem. Soc.* **115,** 6277 (1993).
23. Benson, S. W., "The Foundations of Chemical Kinetics," McGraw–Hill, New York, 1960.
24. Darabiha, N., Candel, S. N., Giovangigli, V., and Smooke, M. D., *Combustion Sci. Technol.* **60,** 267 (1988).